JOURNAL OF GEOPHYSICAL RESEARCH, VOL. 110, C06002, doi:10.1029/2004JC002559, 2005

Numerical sensitivity studies on the variability of climate-relevant processes in the Barents Sea

I. H. Harms, C. Schrum, and K. Hatten

Center for Marine and Atmospheric Science, Institute for Oceanography, University Hamburg, Hamburg, Germany

Received 25 June 2004; revised 30 November 2004; accepted 28 February 2005; published 3 June 2005.

[1] The Barents Sea is a key region in the North Atlantic/Arctic Ocean climate system because of the intense ocean-atmosphere heat exchange and the formation of sea ice. The latter process is connected with salt input, so-called "brine release," whereby water masses of Atlantic origin can be transformed into dense shelf bottom waters. To investigate the sensitivity of simulated, climate-relevant processes to different but well-established and realistic initial and boundary data, a high-resolution coupled ice-ocean model is applied to the Barents Sea. The model is based on the Hamburg Shelf Ocean Model and runs on a 7 × 7 km grid, based on the International Bathymetric Chart of the Arctic Ocean topography. The model is initialized with different temperature and salinity data from the Arctic Climate System Study BarKode data set and is forced with National Centers for Environmental Prediction atmospheric data. Eight sensitivity experiments with initial and boundary conditions in different combinations are performed over a period of 6 years (1979–1984). Results are analyzed with special emphasis on the ocean-atmosphere heat exchange, the ice extent, and the brine release. The experimental variability is compared to the interannual climatic variability in order to assess the role of different forcing terms for regional climate modeling. Our results show that the experimental variability can be partly of the same order than the interannual variability, which suggests that data uncertainties could easily bias the results of climate variability studies. Modification of the Barents Sea inflow had the strongest effect on model results. The ocean-atmosphere heat flux proved to be the most sensitive parameter to oceanic and atmospheric anomalies, whereas the ice extent and the corresponding salt input is more invariant to different boundary conditions.

Citation: Harms, I. H., C. Schrum, and K. Hatten (2005), Numerical sensitivity studies on the variability of climate-relevant processes in the Barents Sea, *J. Geophys. Res.*, *110*, C06002, doi:10.1029/2004JC002559.

1. Introduction

[2] The Barents Sea is a key region in the North Atlantic/Arctic Ocean climate system. It is dominated by climate-relevant processes such as ocean atmosphere heat exchange, ice formation and water mass transformation.

[3] Because of the isolating year-round ice sheet in the central Arctic, the interaction between ocean and atmosphere is more intense on the shelf than in the deep ocean. On the Barents Shelf, warm and saline Atlantic waters meet with cold polar air masses near the marginal ice zone. In these areas, the oceanic heat loss in winter can reach more than 600 W/m^2 [*Harms*, 1997b] which presents a significant input to the local atmosphere. Owing to strong inflow of relative warm Atlantic water masses at high latitudes, the integral ocean-atmosphere heat loss of the Barents Sea probably exceeds the combined heat loss of the much larger Greenland, Iceland, and Norwegian Seas [*Simonsen and Haugan*, 1996].

[4] The magnitude of the heat flux is still under discussion because estimations on the basis of atmospheric reanalysis data or from ocean transport budgets lead to different results: *Simonsen and Haugan* [1996] calculate from atmospheric data a mean heat loss of 100 W/m^2, respectively 136 TW (terra Watt) for the whole Barents Sea. Oceanic transport derived estimations reveal lower values, in the range of 70 TW [*Gerdes and Schauer*, 1997]. These differences may have their origin in the strong interannual variability of the hydrography of the Barents Sea, which is affected significantly by external forcing. Temperature and salinity anomalies as well as volume transport anomalies propagate with the North Atlantic inflow onto the shelf, which explains the good correlation of the Barents Sea climate index with the NAO index [*Aadlandsvik and Loeng*, 1991; *Loeng*, 1991; *Haugan*, 1999].

[5] Several model studies in the last years investigated the area and most of these studies confirmed a strong interannual and decadal variability of almost all climate-relevant parameters in the Barents Sea [e.g., *Karcher et al.*, 2003; *Maslowski et al.*, 2004]. However, the application of different initial or boundary conditions in these studies (temperature, salinity, sea surface elevation, inflow/outflow,

0148-0227/05/2004JC002559$09.00

atmospheric forcing etc.) presents an obstacle when comparing the model results. Also the quality of model forcing data for regional climate studies can be a problem, especially in higher latitudes where regular observing systems are missing and the interaction with sea ice may lead to several uncertainties. All these points make a distinction between ''natural'' climate variability and forcing-induced, ''artificial'' variability of model results more difficult.

[6] One of the basic questions addressed within this study is therefore the possible impact of forcing uncertainties on model results, with respect to the model's capability for investigating ''natural'' climate variability. This is done by evaluating the sensitivity of model results to the application of different atmospheric forcing data or data modifications. Since we also aim to assess the role of the ocean for a regional climate system like the Barents Sea area, different initial conditions and oceanic boundary conditions were investigated with respect to their impact on climate-relevant processes such as ocean-atmosphere heat flux, ice extent and salt release due to ice formation.

[7] The following chapter describes the applied methods which are based on widely accepted and well established model configurations and forcing strategies.

2. Methods

[8] A regional, coupled ice-ocean circulation model for the Barents Sea is used to perform 8 different multiyear sensitivity experiments. The model simulations are based on 6 yearlong hindcast scenarios forced with National Centers for Environmental Prediction, USA (NCEP) and European Centre for Medium-Range Weather Forecasts (ECMWF) reanalysis data.

2.1. Model Physics

[9] The present model is an application of the Hamburg Shelf Ocean Model (HAMSOM) to the Barents Sea. HAMSOM, has been developed at the Institute of Oceanography, University Hamburg, and was continuously improved during the last 20 years by contributions from different authors. It has successfully been applied to several shelf sea regions to investigate hydro- and thermodynamics. Previous applications to the Barents Sea were dedicated to water mass transformation or pollutant transport [*Harms*, 1997a, 1997b], however, based on much coarser grid resolutions.

[10] The Barents Sea model is based on the HAMSOM application to the North Sea and Baltic Sea [*Schrum*, 1997; *Schrum and Backhaus*, 1999], which is the most recent coupled ice-ocean version of HAMSOM. The performance of this model version with respect to climate variability has been assessed in detail for the North Sea/Baltic Sea region by *Schrum et al.* [2000], *Janssen et al.* [2001], *Schrum and Janssen* [2003], and *Janssen* [2002]. In these previous studies, the model showed the general ability to reproduce climate variability on different time and spatial scales, which justifies consequently the present application to the Barents Sea.

[11] HAMSOM is a 3-D, baroclinic circulation model based on nonlinear primitive equations of motion, invoking the hydrostatic approximation. The equation of continuity serves to predict the elevation of the free surface from the divergence of the depth mean transport. The numerical scheme of the circulation model is semi-implicit and the equations are discretized as finite differences on an Arakawa C grid. Vertical subgrid-scale turbulence is parameterized by means of a turbulent closure approach, proposed by *Kochergin* [1987] and later modified by *Pohlmann* [1996]. Convective overturning is parameterized by a mass conserving vertical mixing scheme.

[12] The ocean model is coupled to a modified Hibler-type [*Hibler*, 1979] thermodynamic and dynamic sea ice model, which calculates space- and time-dependent variations of ice velocities and ice compactness as well as the thickness of level and ridged ice. The dynamic part of the sea ice model uses a viscous plastic rheology described by *Schrum and Backhaus* [1999].

[13] Both model systems, ocean and sea ice model, are coupled thermodynamically and dynamically through the fluxes of momentum, heat and salt. At the ocean-ice-atmosphere interfaces, standard bulk formulae are used for the calculation of sensible and latent heat [*Kondo*, 1975], global short-wave radiation [*Dobson and Smith*, 1988] and wind stress [*Luthardt*, 1987]. Net long-wave radiation is calculated using the Boltzmann radiation formulae, including the emissivity of the atmosphere depending on the cloudiness [*Maykut*, 1986]. Salt fluxes or brine release due to ice formation depend on the thermodynamic ice growth [*Lemke et al.*, 1990].

[14] A detailed list of references and a full description of the most advanced model version, including a coupled sea ice model, which was set up for the North Sea and the Baltic Sea can be found in the work of *Schrum and Backhaus* [1999].

[15] The Barents Sea model has a horizontal resolution of 7×7 km with 16 levels in the vertical. The upper 40 m of the water column are resolved with 5 layers of 8 m thickness. Between 40 m and 215 m depth, the layer thickness is set to 25 m. Larger depths are resolved much coarser, with a layer thickness between 50 and 100 m.

[16] The model domain (Figure 1) covers the whole Barents Sea and the White Sea from roughly 16°E to Novaya Semlya. A coordinate transformation allows for an almost equidistant grid. The northern boundary of the model is marked by a line from the northern tip of Novaya Semlya to the southern tip of Franz-Josef-Land and further to Svalbard. The model topography is extracted from the 2.5 km digital data of the International Bathymetric Chart of the Arctic Ocean (IBCAO [*Jakobsson and IBCAO Editorial Board Members*, 2001]) and interpolated to the 7 km model grid. Since the code of HAMSOM allows for ''partial cells'' in the bottom layer, there is no smoothing of topographic data except the weighted interpolation from the 2.5 km IBCAO grid on the 7 km model grid.

2.2. Initial and Boundary Conditions

[17] Vertical atmospheric boundary conditions are deduced from 6 hourly NCEP [*Kalnay et al.*, 1996] and ECMWF [*Gibson et al.*, 1997] reanalysis data. The following parameters are used: 2 m air temperatures, air pressure, wind speed in 10 m, specific humidity in 2 m or dew point temperature, precipitation and long- and short-wave radiation. These data are used in bulk formulae to calculate the vertical fluxes of heat, moisture and momentum.

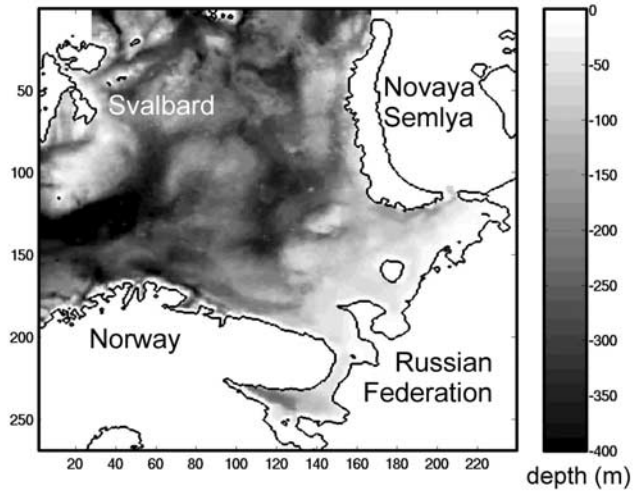

Figure 1. Model domain and topography of the Barents Sea (7 × 7 km).

[18] Horizontal open boundary conditions and the initial conditions for temperature and salinity consist of monthly mean climatological data extracted from the Arctic Climate System Study (ACSYS) Barents and Kara Seas Oceanographic Database BarKode (WRCP/ACSYS Office, Tromsoe, Norway). For this purpose, all available *T-S* profiles from 1900–2000 were collected. The profiles were ordered by month and interpolated first on a regular 50 × 50 km grid and finally on the 7 × 7 km model grid. Larger gaps in the northern Barents Sea had to be filled with model derived climatological databased on the observational period 1949–1999 [*Marsland et al.*, 2003].

[19] Prescribed sea surface elevations at the open boundaries consist of 6 hourly nontidal data values from a regional North Atlantic/Arctic Ocean model (C-HOPE [*Marsland et al.*, 2003]) together with amplitudes of the semidiurnal lunar tide (M_2) from a large-scale tidal model of the world ocean [*Zahel et al.*, 2000]. Like the regional Barents Sea model, the North Atlantic/Arctic Ocean C-HOPE model is forced with atmospheric NCEP reanalysis data. The model physics of C-HOPE are very similar to the HAMSOM code. It is a 3-D, level type model based on nonlinear primitive equations of motion, discretized as finite differences on an Arakawa C grid. The North Atlantic/Arctic Ocean C-HOPE model provides only the sea surface elevations to the Barents Sea model. The tidal solution in terms of amplitudes and phases is also validated and proves to agree well with observations and other tidal models.

[20] There is no explicit ice flux prescribed through horizontal open boundaries. Instead we use a zero-gradient condition normal to the boundary, which allows ice to leave the domain or to enter when ice is present at the lateral boundary.

[21] At the land boundaries, climatological monthly mean river runoff is prescribed from 4 major rivers emptying into the Barents Sea: Petschora, Mesen, Dwina and Onega (R_ArcticNET, A Regional, Hydrometeorological Data Network for the pan-Arctic Region, http://www.r-arcticnet.sr.unh.edu/abstract.html). The volume fluxes are prescribed in m^3/s at the grid point where the river enters the sea. At these points the salinity is kept to zero.

2.3. Model Experiments

[22] The above described model configuration was used to carry out a variety of experiments in order to simulate the low-frequency variability of climate-relevant processes in the ice-ocean-atmosphere system and their sensitivity to initial and boundary conditions. All model experiments were run for 6 years, from 1979 to 1984. For spin-up, the model was integrated four months with NCEP 1978 data starting in the ice-free period on 1 September. The start of the sensitivity runs is 1 January 1979.

[23] The configuration of the model experiments represent a compromise between high model resolution, number of sensitivity runs and length of the simulation period. Although a 6 year simulation period seems to be quite short when looking at climate scales, we feel that this time span is reasonable because it is approximately twice as long as the average flushing time of the Barents Sea. This means that the model is able to adapt to different initial conditions or to perturbations in the external forcing.

[24] The set of experiments comprise A-experiments dedicated to the testing of different atmospheric forcing and O-experiments to investigate the influence of oceanic anomalies on regional climate-relevant processes (Table 1).

2.3.1. Configuration of the A-Experiments

[25] These experiments refer to four different realizations of atmospheric forcing. We applied the uncorrected NCEP data and three different correction methods using ECMWF

Table 1. Configuration of Sensitivity Experiments Performed With the Barents Sea Model[a]

		Experiment Code							
Forcing Type	Experiment Configuration	O1	O2	O3	O4	A1	A2	A3	A4
Atmospheric Forcing	NCEP					X			
	NCEP constant correction	X	X	X	X		**X**		
	NCEP regional correction							X	
	NCEP correction from SST								X
Open boundaries	*T-S* climatology	X		X	X	X	**X**	X	X
	T-S anomaly GSA		X						
	enhanced transport BSO	X							
	M2 tide				X				
Initial *T-S* conditions	initial climatological *T-S* data	X	X		X	X	**X**	X	X
	initial real data (September 1978)			X					

[a]Hindcast period is from 1979 to 1984; the reference run is in boldface. Abbreviations are as follows: NCEP, National Centers for Environmental Prediction; SST, sea surface temperature; GSA, Great Salinity Anomaly; BSO, Barents Sea opening.

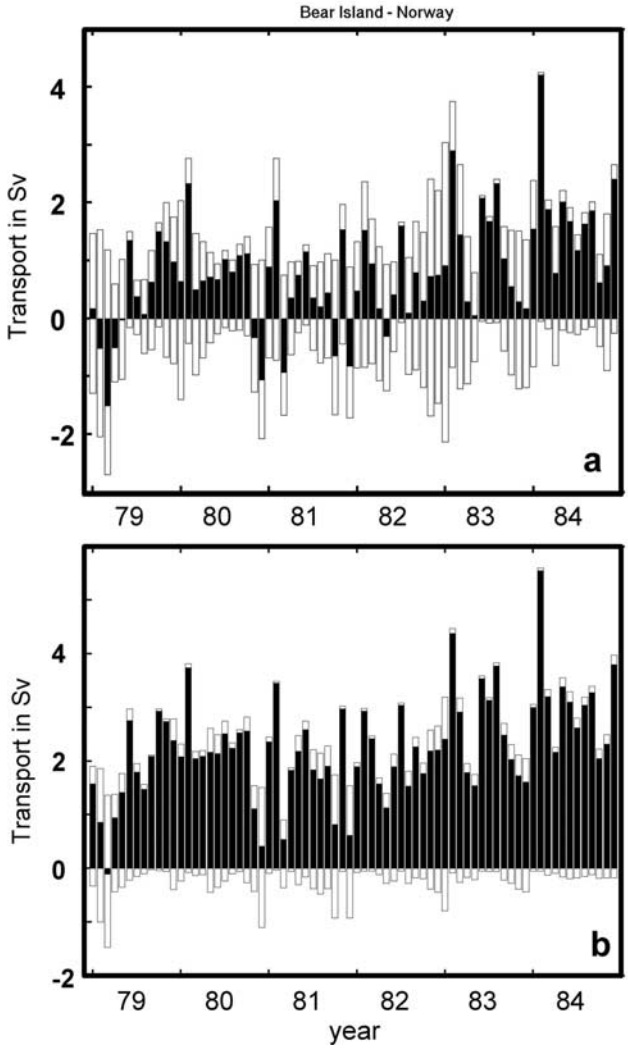

Figure 2. Time series of transport rates in Sv (Sverdrup = 10^6 m^3/s) through the Barents Sea opening (white columns) for (a) the reference experiment A2 and (b) the increased throughflow experiment O1. The net throughflow in both experiments is shown in black.

reanalysis data for the same period. The configuration of the A-experiments is as follows.

[26] A1. Application of uncorrected NCEP reanalysis data.

[27] A2. Application of NCEP reanalysis data and correction of incoming short-wave radiation by factor 0.89. Background of this experiment is the fact that NCEP data overestimate the incoming solar radiation globally by roughly 11% [*Semmler*, 2002] compared to ECMWF data which leads to uncertainties in the reproduction of the sea ice cover found for example in regional models for the Baltic Sea [*Schrum and Janssen*, 2003].

[28] A3. Application of NCEP reanalysis data using a regional, monthly correction of NCEP air temperatures, short- and long-wave radiation. For this correction, we deduced climatological monthly mean values from NCEP and ECMWF data for all three parameters over a period where both data sets are available (1 December 1978–1 March 1994). The differences NCEP – ECMWF were interpolated to the model grid and used to correct the NCEP forcing.

[29] A4. Correction of the long-wave radiation according to the simulated sea surface temperature (SST). In this experiment, the short-wave radiation is taken from NCEP data and applied like in A2, however, the long-wave radiation is not taken from NCEP. Instead, we used the simulated SST to compute long-wave radiation fluxes, which allows mesoscale structures at the sea surface and in the ice cover to be reflected in the heat flux patterns.

[30] Apart from the specifications given above, all A-experiments were forced with boundary and initial conditions from climatological temperature and salinity data and with C-HOPE model derived daily sea surface elevations. Tides were not considered within the A-experiments.

2.3.2. Configuration of the O-Experiments

[31] These 4 sensitivity experiments refer to oceanic boundary conditions or oceanic anomalies. The basic configuration is according to the A2-experiment, which serves therefore as reference run. The specification of the O-experiments is as follows.

[32] O1. Application of increased transport rates through the Barents Sea opening (BSO). The analysis of the A2 run shows that the yearly mean Barents Sea net throughflow is partly below 1 Sv (Sverdrup = 10^6 m^3/s) (Figure 2a) which is clearly too low compared to published values [e.g., *Karcher et al.*, 2003; *Maslowski et al.*, 2004]. We therefore enhance in this experiment the sea surface gradient along the lateral boundary and increase the geostrophic inflow through the Barents Sea opening by roughly 1.5 Sv so that the average net throughflow is in a range of 2–3 Sv (Figure 2b).

[33] O2. Application of a temperature (T) and salinity (S) anomaly. In this experiment, the *T-S* characteristic of the North Atlantic inflow through the Barents Sea opening is modified by prescribing a cold and less saline anomaly ($dT = -1°C$; $dS = -0.1$) to the western open boundary. This experiment refers basically to the consequences of the Great Salinity Anomaly (GSA), which was observed in that area during the 1970s [*Belkin et al.*, 1998].

[34] O3. Modification of the initial *T-S* conditions. The initial climatological field of temperature and salinity from A2 is replaced in O3 by observed data from September 1978, which presents the starting month of all sensitivity experiments. These data were deduced in a similar way like the climatological data from the ACSYS/BarKode data set.

[35] O4. Inclusion of the semidiurnal lunar tide M_2 in the reference run A2 by forcing the open boundaries with amplitudes and phases deduced from a global tidal model (see above).

3. Model Results

[36] Prior to the assessment of the model's experimental sensitivity to different initial and boundary conditions, the reference run was evaluated and the inherent "natural" climate variability was analyzed. Several comparisons with observations showed that the model results are close to reality and represent sufficiently well the seasonal and interannual variability. A further detailed model validation, however, is omitted at this point because it would be out of

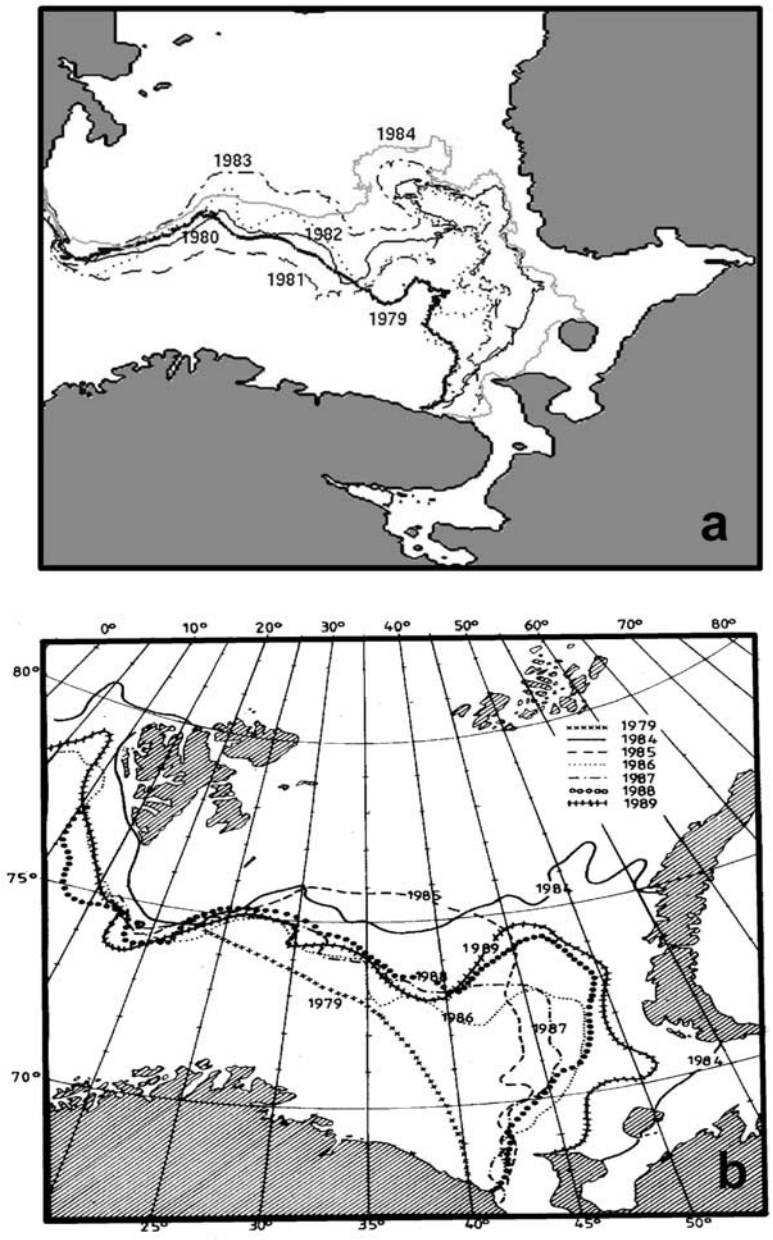

Figure 3. (a) Simulated and (b) observed ice edge [*Loeng*, 1991] during the hindcast period 1979–1984.

scope of this study. Instead, the performance of the model is demonstrated only very briefly for two important variables:

[37] The simulated annual mean oceanic heat loss to the atmosphere of all experiments ranges between 46 and 102 TW for the hindcast period with a mean value of 61 TW. However, mean values for individual experiments can be very different. The highest annual mean heat loss was found to be of 73 TW (O1), the lowest 54 TW (O2). These values are smaller than the values given by *Simonsen and Haugan* [1996] (∼136 TW) but in good agreement with *Gerdes and Schauer* [1997] who estimated a range of 60–80 TW.

[38] Another important climate-relevant parameter is the ice extent. A comparison between observed and simulated maximum ice edges (Figure 3) shows that the model is able to reproduce the interannual variability very well, including the extreme high 1978/1979 and extreme low 1983/1984 winter ice coverage.

[39] In the following subsections, the model results will be presented separately for the O- and the A-experiments. For both categories, we analyze the time and spatial variability of ocean-atmosphere heat flux, ice extent and resulting salt input due to freezing.

3.1. Results From the O-Experiments

3.1.1. O-Experiments: Heat Fluxes

[40] All sensitivity runs of this category show an intense reaction of the ocean-atmosphere heat flux to modifications

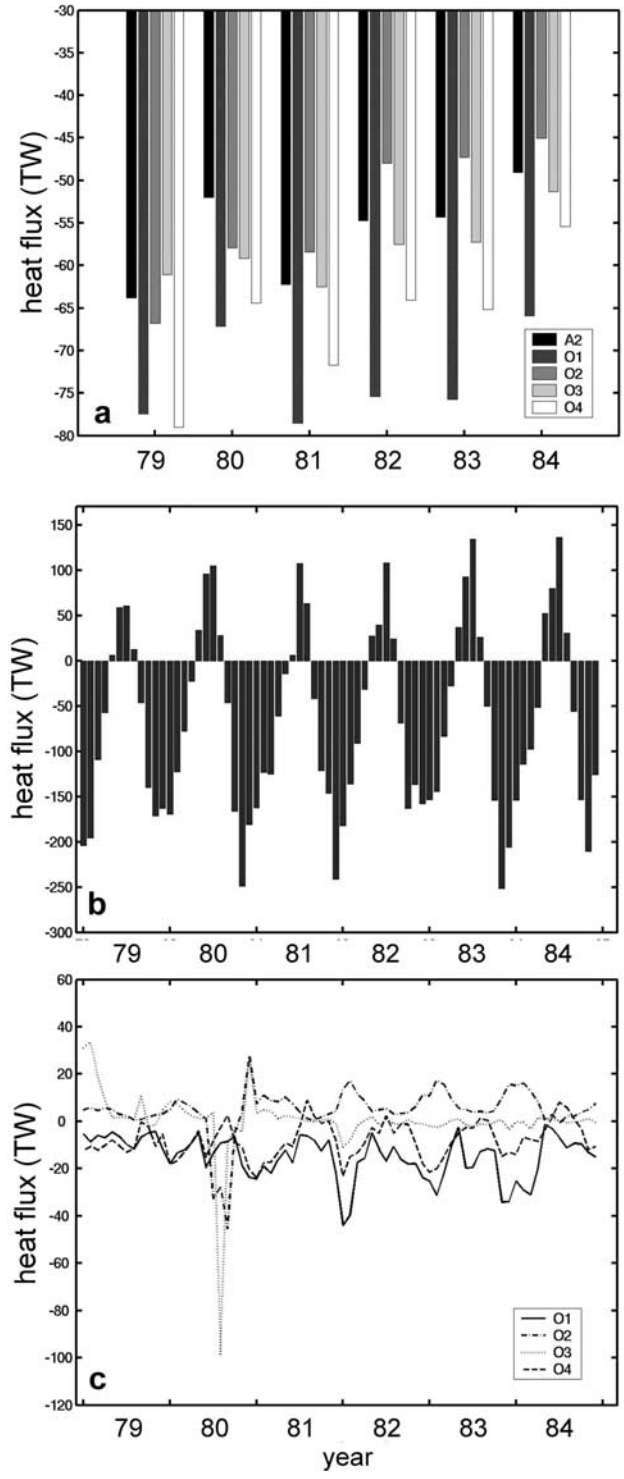

Figure 4. (a) Annual mean heat flux (TW) for different O-experiments, (b) monthly mean heat flux of the reference run A2, and (c) monthly mean oceanic heat flux differences: O-experiments minus reference run A2 (Ox – A2). Negative heat flux in Figures 4a and 4b equals ocean heat loss to the atmosphere; positive heat flux equals ocean heat gain from the atmosphere.

of initial and boundary conditions. The yearly mean heat flux of the O-experiments is negative (i.e., oceanic heat loss) and ranges between −46 and −78 TW (Figure 4a) with a mean value for the hindcast period of −73 TW (O1), −53 TW (O2), −58 TW (O3) and −66 TW (O4). The reference run A2 shows an annual mean value of −58 TW.

[41] Yearly mean heat flux differences between A2 and the O-experiments partly exceed 20 TW (e.g., in 1982 and 1983), which is in the same range or even higher than the interannual variability. However, in this respect there is a clear hierarchy in the O-experiments: A stronger but more realistic inflow through the Barents Sea Opening (O1) leads to a negative heat flux anomaly between 10 and 20 TW which corresponds to an increase of the oceanic heat loss of roughly 25%. Monthly mean differences to the heat fluxes of A2 (Figures 4b and 4c) show that the heat loss increase is not a simple bias but modulates the intensity of the seasonal and interannual variability. The increase of oceanic heat loss is strongest during autumn and winter when the Atlantic inflow is strongest. The differences are small in spring and early summer, when the heat loss is low due to a larger ice cover.

[42] Second in the hierarchy of heat flux differences is experiment O4, which includes the M_2 tide. Owing to tidal currents and enhanced mixing, more heat from the ocean interior is brought to the surface so that the yearly averaged heat flux is more negative than in A2. The difference corresponds to a heat loss increase of roughly 15%. However, these effects can be regionally very different. The influence of tidal stirring on the heat loss is in particular stronger close to the Polar Front, along the marginal ice edge and in shallow shelf areas. The Polar Front southeast of Svalbard is a marked discontinuity in surface temperature and salinity. It separates cold, less saline Arctic surface waters from waters of Atlantic origin. The ice edge in winter coincides frequently with the Polar Front. In these areas, tidal mixing affects the vertical stratification of the water column and horizontal gradients.

[43] The initial field (O3) has a pronounced influence within the first 2 years. Differences to A2 show much higher positive heat fluxes in 1979, followed by much lower negative values in autumn 1980. However, the difference levels out to almost zero during the following 4 years. This basically confirms previously estimated flushing times for the Barents Sea of 2.5–3.8 years for deeper regions (>200 m) and 1.1–4.5 years for the shallow parts [*Harms*, 1994].

[44] The only simulation where the annual mean heat flux is constantly higher (i.e., less negative) than in the reference run is O2, the application of a GSA-similar *T-S* anomaly in the Barents Sea Opening. The primary effect is that due to lower sea surface temperatures, the oceanic heat loss decreases. A larger ice cover causes a secondary effect in winter, which inhibits the heat exchange between ocean and atmosphere. This reduces the heat loss particularly in autumn and winter as could be seen in Figure 4c. The enhanced ice extent is due to lower temperatures but in particular also due to lower salinities. Fresher surface water facilitates ice formation mainly by stabilizing the water column but also by raising the freezing point temperature although this latter contribution might be very small compared to the first one.

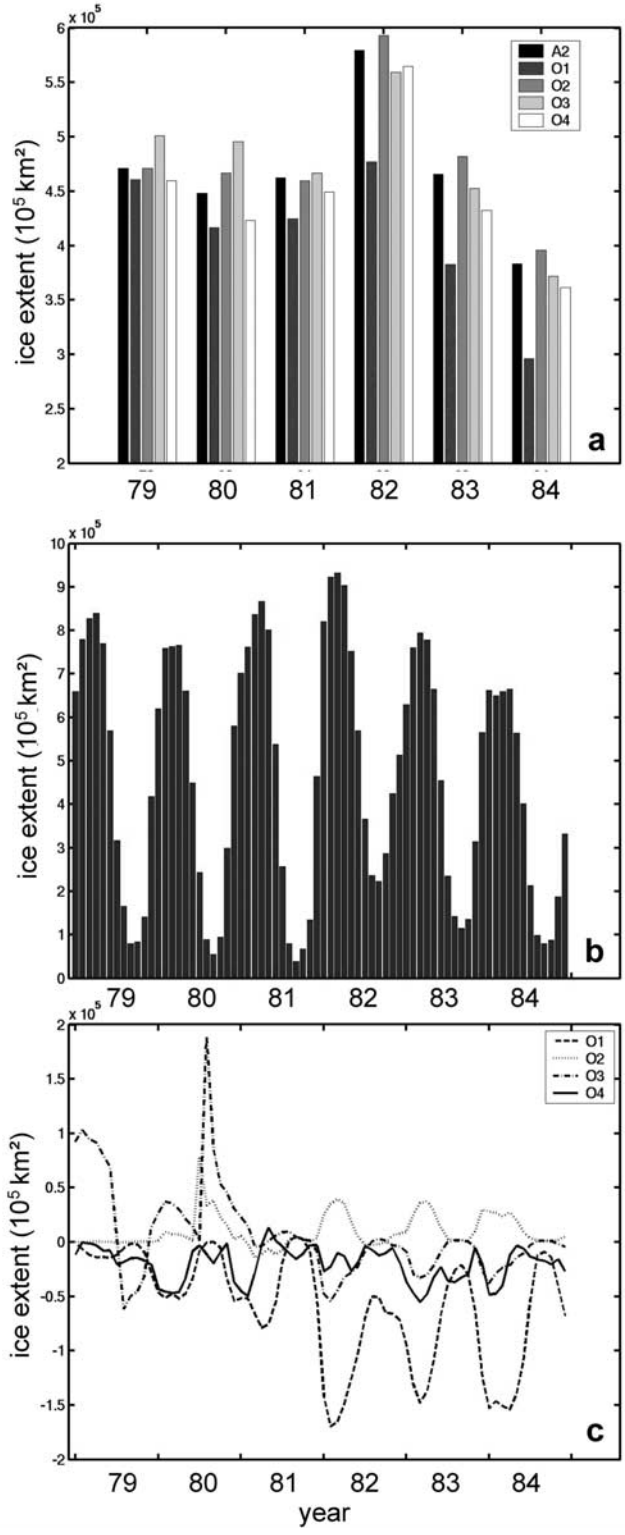

Figure 5. (a) Annual mean ice extent (10^5 km^2) for different O-experiments, (b) monthly mean ice extent of the reference run A2, and (c) monthly mean differences in ice extent: Ox – A2.

3.1.2. O-Experiments: Ice Extent

[45] In general, the influence of oceanic anomalies on the seasonal ice cover is less intense than on the heat flux (Figure 5a). The yearly mean ice extent, averaged over the hindcast period, ranges between 4.1×10^5 km^2 (O1) and 4.8×10^5 km^2 (O2) with the reference run A2 being at 4.6×10^5 km^2. The maximum ice cover (Figure 5b) has an area of $7–9.5 \times 10^5$ km^2 which corresponds to an interannual variability range of $2–2.5 \times 10^5$ km^2 for the hindcast period. Monthly mean differences of the O-experiments to the reference run (Figure 5c) remain clearly below these values for most of the experiments.

[46] The most intense response of the sea ice extent shows up in the experiment O1 (transport increase) followed by O3 (initial conditions). The inflow enhancement in the O1-experiment leads to a seasonally modulated decrease of the ice cover in the Barents Sea. The winter ice extent is strongly affected by this experiment whereas the summer ice extent shows a much smaller deviation from the reference run. As could be expected, the presence of warmer and saltier water masses enforces and prolongs thermal convection in autumn, which hampers the ice formation in early winter. This effect does not show up instantaneously because of the advective timescales. The ice cover therefore decreases gradually from 1979 on, showing a very pronounced minimum in winter 1982, which again confirms flushing times of 2–3 years.

[47] Apart from these thermohaline processes, there is also a dynamic effect in O1. A stronger Atlantic inflow moves the Polar Front in the central Barents Sea farther northward, which in turn affects the position of the ice edge (Figure 6). The O1 ice edge shows therefore a much smaller deviation from the reference run in freshwater dominated coastal areas in the southeast Barents Sea, where the Atlantic influence is small. Both Figures 5 and 6 reveal that the deviation of the other O-experiment results from the reference run is rather small. The O3-experiment (initial conditions) shows, like with the heat fluxes, a stronger reaction in the first two years but only very small differences during the remaining period. A striking feature in

Figure 6. Maximum ice extent in winter 1983/1984 for the reference run A2 and O-experiments.

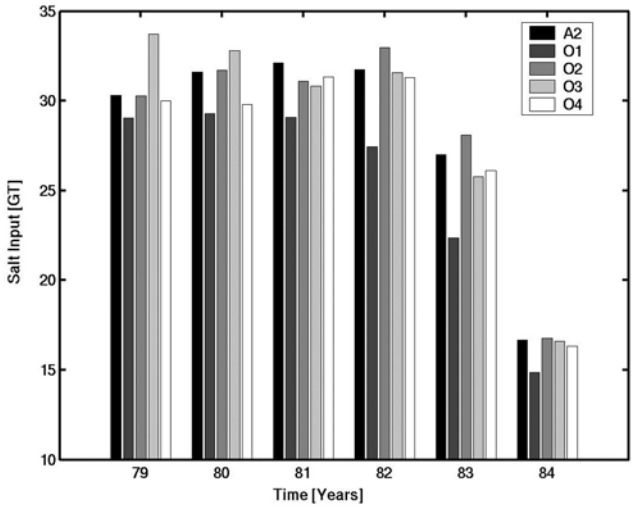

Figure 7. Annual mean salt input (GT) for different O-experiments.

Figure 5c is the much larger ice extent in autumn 1980, which follows the negative heat flux anomaly visible in Figure 4c.

[48] The O2 run (GSA) is the only simulation within the O-experiments that shows more or less constantly a larger ice cover, in particular during winter (Figure 5c). The deviation of the O4-experiment (tides) from the reference run is marginal. However, Figure 6 reveals that tides tend to smooth frontal structures, which is visible along the Polar Front near Bear Island and also in the central Barents Sea.

3.1.3. O-Experiments: Salt Input

[49] Seasonal sea ice formation is connected with the rejection of salt or "brine release" which is an important process in the Barents Sea in terms of water mass transformation. Large amounts of dense bottom water are formed in polynias, recurrent wind-induced openings in the ice cover along coasts or islands. These areas can be found frequently in the Barents Sea, south of Franz-Josef-Land, around Svalbard and along the west coast of Novaya Semlya. Polynias are characterized by strong heat loss and ice formation, which leads to intense salt release. These processes are assumed to be highly variable in space and time. However, the following discussion considers first of all the integral effect, i.e., the spatial averaged salt input for the whole Barents Sea.

[50] The yearly mean salt input for the hindcast period 1979–1984 (Figure 7) sums up to 25 GT (giga tons = 10^6 tons) for O1, 28 GT (O2), 28 GT (O3) and 27 GT (O4). For comparison: 30 GT corresponds to a virtual salinity increase of roughly 2.7 psu in an 8 m surface layer.

[51] The year-to-year variability of the salt input is very small during the first four years from 1979–1982. In this period, the experimental variability caused by different open boundary conditions is clearly larger than the interannual variability. This changes drastically from 1982 to 1984, due to a significant decrease in ice formation and salt input for all experiments. During these last three years, the year-to-year variability clearly dominates the experimental variability.

[52] The reduced ice formation and salt input can be partly attributed to the Atlantic inflow through the Barents Sea opening. In fact, the period 1982–1984 is characterized by a stronger Atlantic inflow and a rather warm temperature anomaly in the Barents Sea opening [*Furevik*, 2001; *Karcher et al.*, 2003]. However, since the model is forced with climatological data at the Barents Sea opening, it is only the enhanced inflow that can serve as an explanation for reduced ice formation and salt input.

[53] In general, Figure 7 shows that a cold and less saline anomaly (O2) enhances the salt input due to stronger ice formation whereas the increased Barents Sea inflow (O1), which can be regarded basically as a warm and saline anomaly, has a contrary effect, however, much stronger. Using the initial T,S field from 1978 (O3) leads to enhanced ice formation, which in turn increases the salt input. Again, this effect fades after 2–3 years and levels out to almost zero. The overall tidal effect on the salt input (O4) is very small and slightly negative. It remains under 6% of the A2 values.

3.2. Results From the A-Experiments

3.2.1. A-Experiments: Heat Fluxes

[54] The A-experiments are focused on modifications of short- and long-wave radiation and turbulent heat fluxes. In

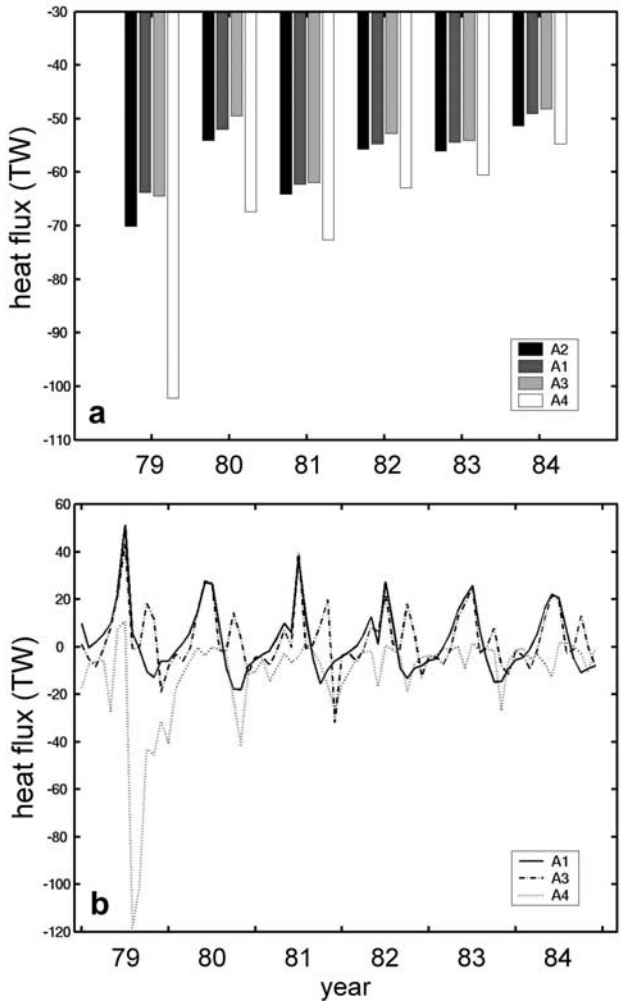

Figure 8. (a) Annual mean heat flux (TW) for different A-experiments and (b) monthly mean heat flux differences: Ax – A2.

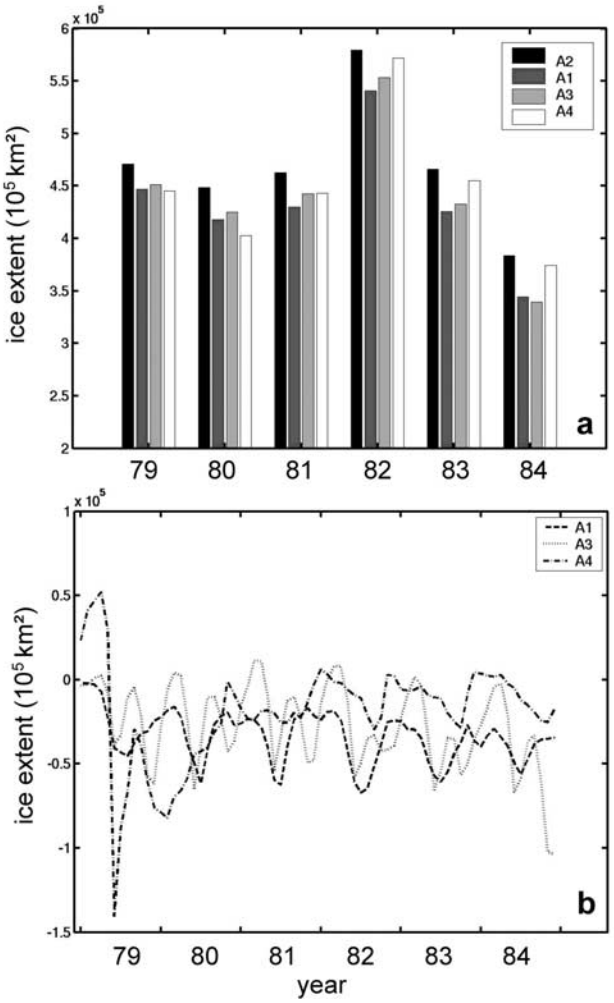

Figure 9. (a) Annual mean ice extent (10^5 km^2) for different A-experiments and (b) monthly mean differences: Ax – A2.

these experiments, the yearly mean oceanic heat loss is generally less affected than in the O-experiments, however, apart from the A4-experiment. The yearly mean averaged heat flux of all A-experiments (Figure 8a) ranges between −50 and −102 TW with a mean value for the hindcast period of −56 TW (A1), −59 TW (A2), −55 TW (A3) and −70 TW (A4).

[55] A significant influence on the overall heat balance is visible for the A4-experiment, where the long-wave radiation is calculated on the basis of the simulated SST. At the beginning of the simulation, the yearly mean heat flux is about 30 TW lower than in the reference run. This value decreases in the following two years to 13 and 10 TW, respectively and finally goes down to 4 TW difference, compared to the reference run.

[56] The enormous deviation at the beginning of the A4-simulation is due a mismatch between the climatological, initial SST and "real" situation in 1978–1979. In that time, the Barents Sea was in a quite cold state as an effect of the *GSA* during the 1970s [*Loeng et al.*, 1993; *Belkin et al.*, 1998] and the applied climatological SST is significantly higher than the "real" SST during that time which served as basis for the NCEP analysis. As a consequence, the long-wave radiation and the turbulent heat fluxes are much lower (more negative) in the beginning of this experiment compared to the NCEP data. Although this effect ceases when the model adapts to the real conditions, the initial difference between A4 and the control run A2 is the highest within the A-experiments. This result underlines the importance of consistent data sets and points toward coupled ocean-atmosphere models also for regional applications in order to include the feedback between ocean and atmosphere.

[57] The yearly mean differences between A1, A2 and A3 are fairly small. The constant correction in A2 leads to a 3–5 TW stronger heat loss than with the uncorrected NCEP forcing (A1). The more complex correction in A3 shows the smallest difference for the yearly mean heat flux. A reason for this similar behavior can be found in the nature of radiation in high latitudes. Since the short-wave heat flux dominates in summer and the long-wave in winter they might cancel out in yearly mean budgets, especially if a systematic error (e.g., underestimated cloud cover) occurs.

[58] In fact, monthly mean heat flux differences (Figure 8b) show a strong modulation of the seasonal variability. The A1 heat flux differences are positive in summer (i.e., more heat gain), when the ice cover is small and large parts of the ocean are exposed to incoming solar radiation. The differences are negative (i.e., more heat loss) in winter when atmospheric cooling is dominating. The underestimated cloud cover of A1 thus leads to small yearly mean differences but distinct seasonal modulations.

[59] The A3-experiment behaves very similar: positive differences in summer denote more heat gain whereas negative differences in autumn and winter denote more heat loss compared to A2. This implies that the more sophisticated corrections in A3 (seasonal and regional correction factor according to ECMWF) seem to cancel out which leads to a similar heat flux behavior like with the uncorrected forcing of A1. However, a systematic difference occurs in late summer and autumn when A3 shows positive heat flux anomalies whereas A1 reveals negative anomalies. This deviation is probably a result of the different ice cover that underlies the ECMWF and NCEP data. A totally different behavior is visible for the A4-experiment, where in autumn 1979 and partly also in autumn 1980 due to the higher simulated SST (see before) the heat flux shows a very pronounced negative anomaly.

3.2.2. A-Experiments: Ice Extent

[60] In all A-experiments, the summer ice cover is smaller than in the reference run (Figure 9a), which is in case of A1 due to higher (uncorrected NCEP) incoming solar radiation. This provides on average a stronger heat gain (compare Figures 8a and 8b), which consequently reduces the ice cover in A1. In A3, the solar radiation is reduced by similar factors like in A2, which should result in similar ice extent. However, the ice extent of A3 remains smaller than in A2. This is due to the fact that in A3 the long-wave radiation and the turbulent heat fluxes are also modified according to ECMWF data. These modifications partly compensate the reduction of the short-wave radiation by providing additional heat, mainly during the summer months (c.f. Figure 8b). The smaller ice extent of A3 compared to A2 is thus particular strong in summer as Figure 9b reveals whereas the winter deviations are close to neutral. The same

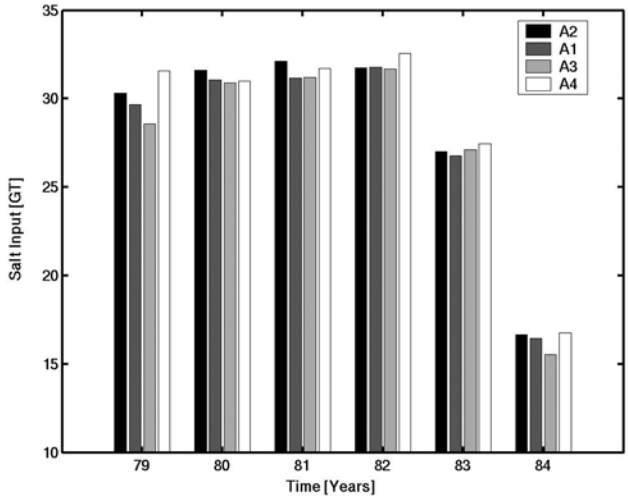

Figure 10. Annual mean salt input (GT) for different A-experiments.

holds true for the A1 deviations. However, in this experiment also the winter deviations remain negative.

[61] The A4 ice extent deviation shows a similar disturbance in the first two years like the heat flux curve did. Following a positive anomaly in spring 1979, the ice extent drops to a pronounced negative anomaly in summer 1979. Since the differences level out in the following years, the initial disturbance can be attributed to the mismatch between simulated SST and NCEP data as outlined before. In general, the amplitudes of the ice cover differences in A-experiments are less than half of the values simulated in the O-experiments.

3.2.3. A-Experiments: Salt Input

[62] Yearly mean experimental differences of the salt input in the A-experiments (Figure 10) are small compared to those from the O-experiments (compare Figure 7). The individual yearly mean salt input sums up to 28 GT (giga tons = 10^6 tons) for A1, 28 GT (A2), 27 GT (A3) and 29 GT (A4). This suggests a very small variability induced by the applied corrections of atmospheric forcing. A modification of radiative heat fluxes affect first of all the onset of ice freezing and melting in autumn and spring. This is particular important at the ice edge and in polynia areas. However, yearly mean and spatially averaged values as presented in this study do not reflect the seasonal and the regional variability, which is supposed to be very pronounced for this parameter.

4. Discussion

[63] In Figure 11, the absolute magnitude of individual deviations from the reference run, averaged over the whole hindcast period is depicted. It is obvious from this figure that the largest deviations (up to 25%) occur with the heat flux budget, followed by the salt input and the ice extent.

[64] The main reason for this behavior is the strong dependence of the heat flux parameter from the temperature difference between ocean and atmosphere. The negative heat flux budget of the Barents Sea (compare Figures 4a and 4b) is caused mainly by turbulent and long-wave radiative heat fluxes that depend on ocean-atmosphere temperature differences. Therefore all experiments that imply a significant modification of the SST (O1, "BO inflow"; O4, "tidal mixing"; and A4, "SST-based long-wave radiation") show a rather strong response in the heat flux budget. It has to be mentioned, that the strong heat flux reaction of A4 in Figure 11 (~20%) is mainly a result of the first two years where the initial shock from the simulated SST (see before) leads to enormous deviations from the reference run. As outlined before, this effect decreases when the model adapts to the modified conditions.

[65] Deviations of the yearly mean ice extent and salt input remain usually below 5% and 10%, respectively. In contrary to the direct heat flux response, these processes evolve more slowly because they depend not only on temperature differences or heat fluxes but also on the ocean's preconditions, i.e., the vertical stratification. The response of ice formation and salt release is therefore weaker and shows up only if the heat flux deviations are strong and long lasting (e.g., O1).

[66] Modifications of the short-wave radiation (A1, A3) seem to be of minor importance for the heat fluxes (approximately 5% deviation) because the impact of this parameter on the total heat flux balance is small and limited to the spring and summer season. However, the ice extent is significantly affected in A1 and A3. In particular in the A1 run, the ice extent deviation is the second highest and larger than the corresponding heat flux deviation. Since the short-wave radiation is the main driver for the onset of melting in spring, it affects the summer ice extent and prolongs or shortens the ice-free season. We also expect strong regional differences for the ice formation and the salt input if the short-wave radiation is modified. However, an assessment of the regional variability is out of scope of the present paper, which is focused on the integral effect of different forcing strategies for the Barents Sea region.

[67] In order to assess the experimental variability in relation to the "natural" interannual variability, we calculated mean values and standard deviations for each experiment

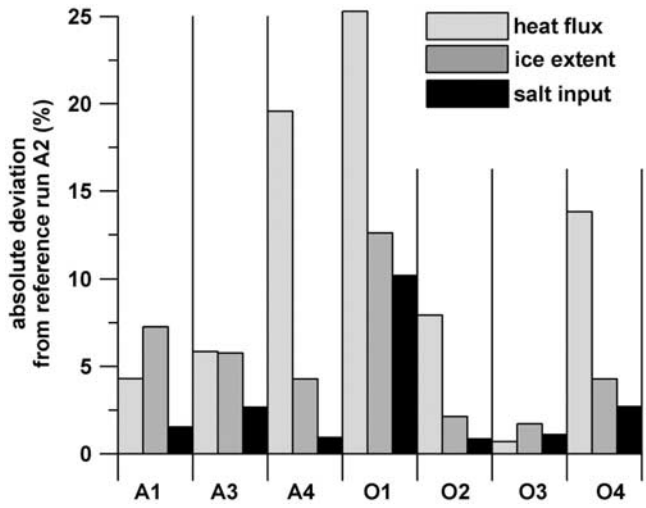

Figure 11. Absolute deviation of the annual mean heat flux, ice extent, and salt input of all sensitivity runs compared to the reference run A2.

Table 2. Relation Between the Experimental and the Interannual Standard Deviations $S_{(experiment)}/S_{(year)}$

	Heat Flux	Ice Extent	Salt Input
O-experiments	1.41	0.54	0.48
A-experiments	0.76	0.26	0.09

over all years, $S_{(year)}$, and for each year over all experiments, $S_{(experiment)}$. This averaging was done separately for all three parameters, annual mean heat flux, ice extent and salt input (brine release). The relation $S_{(experiment)}/S_{(year)}$ thus gives a measure for the dominating influence of either experimental or climatic variability.

[68] Table 2 presents mean values of $S_{(experiment)}/S_{(year)}$, separately for O- and A-experiments. The values reveal, that the experimental variability of the ice extent and the salt input is generally smaller than the interannual variability of these parameters. However, the heat flux results behave different. In particular in the O-simulations, the experimental variability is significantly higher than the interannual. In this category, the standard deviation of O-experimental variability ranges between 12.1 TW (1983) and 4.4 TW (1980) whereas the interannual variability ranges between 8.5 TW (O2) and 3.9 TW (O3). In the A-simulations, the experimental and the interannual variability of the heat fluxes are of the same range.

[69] The smallest influence of experimental variability is found for the salt input parameter within the A-experiments. The mean standard deviation for experimental variability in this category is 0.6 GT which has to be compared to an interannual variability deviation of 5.9 GT. However, the dominance of the interannual variability is first of all an effect of the dramatic decrease in the salt input from 1982 to 1984.

[70] Table 2 shows furthermore that the experimental variability is generally stronger in the O-experiments than in the A-experiments which implies that the O-modifications have a stronger influence on the results. Since the A-experiments refer mainly to uncertainties from the radiation heat fluxes we conclude that these local modifications are less important than the advection of oceanic anomalies. An exception to this statement is the long-wave radiation, which presents during winter an important negative component in the heat flux balance. The correct reproduction of the long-wave radiation, by considering the simulated instead of a databased SST (A4), caused the second highest deviation in the heat flux budgets and changed also ice extent and salt input significantly (compare Figure 11).

5. Summary

[71] The goal of this sensitivity study is not to find the most realistic model configuration but to assess the variability of model results and to highlight the implications for climate modeling of the Barents Sea. The model findings can be summarized as follows:

[72] 1. Although the mean experimental variability is generally smaller than the interannual, our results indicate that uncertainties in oceanic or atmospheric forcing conditions may easily bias the results of simulated interannual variability in the Barents Sea. This concerns in particular the seasonal modulation of climate-relevant parameters.

[73] 2. The strongest deviation from the reference run (25% for the yearly mean heat flux) and a clear dominance of experimental variability can be observed for the modification of the Barents Sea inflow (O1) which underlines the enormous importance of advective transport and *T-S* anomalies at the western boundary of the Barents Sea. Model results depend very much on these parameters and modeling studies should take care for its realistic reproduction.

[74] 3. The largest effect within the A-experiments and the second highest deviation from the reference run ($\sim$20% for yearly mean heat flux) is achieved by using the simulated instead of the databased SST for the heat flux bulk formulae. This underlines the importance of consistent data sets in climate modeling and points to the need of coupled regional atmosphere-ocean models for the shelf areas.

[75] 4. Tides seem to play an important role for all climate-relevant parameters in the Barents Sea. The O4-experiment reveals distinct changes in sea ice extent and salt input and causes the third highest deviation in the heat flux budget ($\sim$15%).

[76] 5. Experimental variability caused by a modification of oceanic initial conditions can be very intense. In fact, the highest monthly mean difference in heat flux and ice extent is observed in this category (O3), which bears a high potential for biasing model results. However, the effect is limited to the overall flushing time of the Barents Sea.

[77] 6. The heat fluxes from radiation remain uncertain constituents in the heat flux balance of the Barents Sea because they depend on an uncertain parameter, the cloudiness. Owing to different seasonal dominance of short- and long-wave radiation and the fact that clouds have a contrary effect in both heat flux components they might cancel out in yearly mean budgets, in particular if a systematic error (e.g., underestimated cloud cover) occurs in the data.

[78] The study reveals a significant amount of experimental variability in our sensitivity runs caused by modifications of initial and boundary conditions. For certain modifications, the experimental variability can be even larger than the interannual one which is critical if ocean climate variability is studied. In this respect, it has to be mentioned again that the presently applied modifications of boundary data or initial conditions are not "exotic" but widely accepted and also well-established methods. This underlines that although there has been much progress in the past in the modeling field, forcing and initialization are still crucial points. Even sophisticated state-of-the-art model results are difficult to evaluate or to compare if uncertainties in forcing data and methods are not considered. In particular budget estimations for certain parameters such as ocean-atmosphere heat flux remain critical.

[79] We did not investigate so far the influence of modifications in the wind field mainly because uncertainties are small in this respect. However, wind induced variability in water mass distribution and especially the location of the Polar Front is suggested to be an important process for the interannual variability of sea ice and brine release.

[80] Still an open question is the regional and interannual variability of brine release and the importance of polynia regions for the water mass transformation. Our results show that a realistic approximation of its variability can be expected if the initial and boundary conditions are carefully

chosen. In the present pilot study, however, we excluded the process of water mass transformation from the discussions because this would change the focus of the paper too much. A detailed investigation of this topic is underway.

[81] **Acknowledgments.** This work was funded by the Deutsche Forschungsgemeinschaft (DFG) in the frame of Sonderforschungsbereich 512, Tiefdruckgebiete und Klimasystem des Nordatlantiks. Many thanks to Michael Karcher, who discussed with us patiently all our findings. Ute Hochbaum helped us very much with all figures. Thanks to two anonymous referees for their helpful comments.

References

Aadlandsvik, B., and H. Loeng (1991), A study of the climatic system in the Barents Sea, *Pol. Res.*, *10*, 45–49.

Belkin, I. M., S. Levitus, J. Antonov, and S. Malmberg (1998), "Great Salinity Anomalies" in the North Atlantic, *Prog. Oceanogr.*, *41*, 1–68.

Dobson, F. W., and S. D. Smith (1988), Bulk models of solar radiation at sea, *Q. J. R. Meteorol. Soc.*, *114*, 165–182.

Furevik, T. (2001), Annual and interannual variability of Atlantic Water temperatures in the Norwegian and Barents Seas: 1980–1996, *Deep Sea Res., Part I*, *48*, 383–404.

Gerdes, R., and U. Schauer (1997), Large-scale circulation and water mass distribution in the Arctic Ocean from model results and observations, *J. Geophys. Res.*, *102*, 8467–8483.

Gibson, J. K., P. Kallberg, S. Uppala, A. Nomura, E. Serrano, and A. Hernandez (1997), ERA description: ECMWF reanalysis project report 1: Project organisation, Eur. Cent. for Medium-Range Weather Forecasts, Reading, U. K.

Harms, I. H. (1994), Numerische Modellstudie zur winterlichen Wassermassenformation in der Barentssee, Ph.D. thesis, Rep. 7, 97 pp., Fachber. Geowissenschaft., Univ. Hamburg, Germany.

Harms, I. H. (1997a), Modelling the dispersion of ^{137}Cs and ^{239}Pu released from dumped waste in the Kara Sea, *J. Mar. Syst.*, *13*, 1–19.

Harms, I. H. (1997b), Watermass transformation in the Barents Sea—Application of the HAMburg Shelf Ocean Model (HAMSOM), *ICES J. Mar. Sci.*, *54*, 351–365.

Haugan, P. M. (1999), Exchange of mass, heat and carbon across the Barents Sea opening, Ph.D. thesis, Univ. of Bergen, Norway.

Hibler, W. D., III (1979), A dynamic thermodynamic sea ice model, *J. Phys. Oceanogr.*, *9*, 815–846.

Jakobsson, M., and IBCAO Editorial Board Members (2001), Improvement to the International Bathymetric Chart of the Arctic Ocean (IBCAO): Updating the data base and the grid model, *Eos Trans. AGU*, *82*(47), Fall Meet. Suppl., Abstract OS11B-0371.

Janssen, F. (2002), Statistical analysis of multi-year hydrographic variability in the North Sea and Baltic Sea: Validation and correction of systematic errors in a regional ocean model (in German), Ph.D. thesis, Fachber. Geowissenschaft., Univ. Hamburg, Germany.

Janssen, F., C. Schrum, U. Hübner, and J. Backhaus (2001), Validation of a decadal simulation with a regional model for North Sea and Baltic Sea, *Clim. Res.*, *18*, 55–62.

Kalnay, E., et al. (1996), The NCEP/NCAR 40-Year Reanalysis Project, *Bull. Am. Meteorol. Soc.*, *77*, 437–495.

Karcher, M. J., R. Gerdes, F. Kauker, and C. Köberle (2003), Arctic warming: Evolution and spreading of the 1990s warm event in the Nordic seas and the Arctic Ocean, *J. Geophys. Res.*, *108*(C2), 3034, doi:10.1029/2001JC001265.

Kochergin, V. P. (1987), Three-dimensional prognostic models, in *Three-Dimensional Coastal Ocean Models*, *Coastal Estuarine Stud.*, vol. 4, edited by N. Heaps, pp. 201–208, AGU, Washington, D. C.

Kondo, J. (1975), Air-sea bulk transfer coefficients in diabatic conditions, *Boundary Layer Meteorol.*, *9*, 91–112.

Lemke, P., W. B. Owens, and W. D. Hibler III (1990), A coupled sea ice–mixed layer–pycnocline model for the Weddell Sea, *J. Geophys. Res.*, *95*, 9513–9525.

Loeng, H. (1991), Features of the physical oceanographic conditions of the Barents Sea, *Pol. Res.*, *10*, 5–18.

Loeng, H., V. Ozhigin, B. Aadlandsvik, and H. Sagen (1993), Current measurements in the northeastern Barents Sea, *Rep. C.M. 1993/C: 40*, 20 pp., Int. Counc. for Explor. of the Sea, Copenhagen.

Luthardt, H. (1987), Analyse der wassernahen Druck- und Windfelder über der Nordsee aus Routinebeobachtungen, *Hamburger Geophys. Einzelschrift.*, *83*, 1–19.

Marsland, S. J., H. Haak, J. H. Jungclaus, M. Latif, and F. Roeske (2003), The Max-Planck-Institute global ocean/sea ice model with orthogonal curvilinear coordinate, *Ocean Modell.*, *5*, 91–127.

Maslowski, W., D. Marble, W. Walczowski, U. Schauer, J. L. Clement, L. Jaclyn, and A. J. Semtner (2004), On climatological mass, heat, and salt transports through the Barents Sea and Fram Strait from a pan-Arctic coupled ice-ocean model simulation, *J. Geophys. Res.*, *109*, C03032, doi:10.1029/2001JC001039.

Maykut, G. A. (1986), The surface heat and mass balance, in *Geophysics of Sea Ice*, edited by N. Untersteiner, *NATO ASI Ser.*, *146*, 395–463.

Pohlmann, T. (1996), Calculating the annual cycle of the vertical eddy viscosity in the North Sea with a three-dimensional baroclinic shelf sea circulation model, *Cont. Shelf Res.*, *16*, 147–161.

Schrum, C. (1997), A coupled ice-ocean model for the North Sea and the Baltic Sea, *NATO ASI Ser., Ser. 2*, *27*, 311–325.

Schrum, C., and J. O. Backhaus (1999), Sensitivity of atmosphere-ocean heat exchange and heat content in North Sea and Baltic Sea—A comparative assessment, *Tellus, Ser. A*, *51*, 526–549.

Schrum, C., and F. Janssen (2003), Decadal variability in Baltic Sea sea ice development: Analysis of model results and observations, paper 72 presented at the Fourth Workshop on Baltic Sea Ice Climate, Norrköping, Sweden, 22–24 May.

Schrum, C., F. Janssen, and U. Hübner (2000), Recent climate modelling for North Sea and Baltic Sea. part A: Model description and validation (in German), *Ber. Zent. Meeres Klimaforsch.*, *Rep. 37*, 59 pp., Univ. Hamburg, Germany.

Semmler, T. (2002), Der Wasser- und Energiehaushalt der arktischen Atmosphaere, Ph.D. thesis, *Rep. 85*, 67 pp., Max-Planck-Inst. für Meteorol., Hamburg, Germany.

Simonsen, K., and P. M. Haugan (1996), Heat budgets of the Arctic Mediterranean and sea surface heat flux parameterizations for the Nordic Seas, *J. Geophys. Res.*, *101*, 6553–6576.

Zahel, W., J. H. Gavino, and U. Seiler (2000), Angular momentum and energy budgets of a global ocean tide model with data assimilation (in Spanish), *GEOS Ensenada*, *20*, 400–413.

I. H. Harms, K. Hatten, and C. Schrum, Center for Marine and Atmospheric Science, Institute for Oceanography, University Hamburg, Bundesstrasse 53, D-20146 Hamburg, Germany. (harms@ifm.uni-hamburg.de; hatten@ifm.uni-hamburg.de; schrum@dkrz.de)